Vol. 61 (2020) No. 2 June n. 204

SEISMIC RESPONSE OF LONG-SPAN DOMES SUPPORTED BY MULTI-STOREY SUBSTRUCTURES

Deepshikha NAIR[1], Yuki TERAZAWA[2], Ben SITLER[1]and Toru TAKEUCHI[3]

[1] Graduate Student, Tokyo Institute of Technology, Tokyo, Japan; nair.d.aa@m.titech.ac.jp; and, sitler.b.aa@m.titech.ac.jp;
[2] Assistant Professor, Tokyo Institute of Technology, Tokyo, Japan; terazawa.y.aa@m.titech.ac.jp,
[3] Professor, Tokyo Institute of Technology, Tokyo, Japan; takeuchi.t.ab@m.titech.ac.jp

Editor's Note: Manuscript submitted 28 April 2019; revision received 15 November 2019; accepted 13 March 2020. This paper is open for written discussion, which should be submitted to the IASS Secretariat no later than December 2020.

DOI: https://doi.org/10.20898/j.iass.2020.204.007

ABSTRACT

This paper investigates the seismic response characteristics of long-span domes. The natural periods of the prominent modes are longer than medium-span domes, which leads to a greater contribution from the higher modes to the response of the long-span dome. The acceleration distributions, particularly the vertical acceleration distributions are sensitive to the dominant mode shapes of these higher modes. This leads to inaccuracies when applying the previously proposed response evaluation methods. The vibration modes of multi-storey supporting substructures also affect the excited vibration modes of the roof. In this paper, the dynamic characteristics and seismic response of 150m-span domes supported by multi-storey substructures are studied. The effects of the post-yield stiffness of multi-storey substructures are also analysed by considering two structural systems, buckling-restrained braced frames (BRBF) and damped spine frames. A simple design procedure to evaluate the equivalent static loads using amplification factors and incorporating the effects of higher modes is proposed based on response spectrum analysis and equivalent linearisation procedures. The accuracy of the proposed method is evaluated by comparing the responses with those obtained from non-linear response history analysis.

Keywords: *Long-span Domes, Equivalent Static Loads, Higher Mode Effects, Spine Frames, Buckling-restrained Braced Frames*

1. INTRODUCTION

The seismic response characteristics of domes are known to be complicated owing to a large number of parallel vibration modes. These characteristics also vary with parameters like the half-subtended angle (and related rise-to-span ratio) and the stiffness of the supporting substructure. Studies conducted by Ogawa et al. [1] found that medium-span dome roofs with some rise are excited not only in the horizontal direction but also experience large anti-symmetric vertical accelerations when subjected to horizontal earthquake ground motions.

In the case of relatively thin lattice domes, a large number of vibration modes with similar periods significantly participate in the response. Nevertheless, it has been observed that when the out-of-plane stiffness of the roof is large, the response characteristics are predominated by fewer modes which are used to present design criteria for the ultimate limit state.

Takeuchi et al. [2] carried out studies to determine the response characteristics of medium-span domes (span~60m) supported by elastic substructure. Amplification factors for the roof were proposed to evaluate the seismic response using response spectrum analysis. Subsequently, the inelastic response of a single-storey substructure was incorporated to present a simplified procedure to evaluate the seismic response of domes using the prominent anti-symmetric vibration mode of the roofs [3].

In the past decade, there has been a rise in the number of long-span steel spatial structures incorporating response control strategies, which has further propelled the need to investigate and present simple design methods for practising engineers. However, the literature is sparse in studies on the seismic response of long-span roofs.

Kato and Nakazawa [4] investigated the response of a 100m single layer reticular dome supported by substructure. They concluded that the two-mode based equivalent linearisation method can accurately predict the response of a certain class of domes that exhibit a substantial substructure sway. However, the effects of higher modes were not so prominent and the effects of the stiffness of a multi-storey substructure on the roof response were outside the scope of that study. An extension of this method was proposed by Kato et al. [5] incorporating the contribution of higher modes. The analysis model was further simplified as a series of parallel lumped masses with elastic springs. This method was found to be accurate for cases where the cumulative mass participation from the first two modes exceeds 90%.

Excessive strength in the substructures often leads to an amplified roof response. Hence, Kato et al. [6] investigated the response of a long-span double-layered dome supported by a single-storey ductile substructure. This study assumed that nonlinearity in the structure is concentrated in the energy-dissipating braces in the substructure. The proposed numerical method estimated equivalent static loads for two seismic intensity levels and was found to be applicable for design of school gymnasiums. An extension of this study to include ductile multi-storey substructures such as large scale stadiums is yet to be conducted.

This paper aims to obtain equivalent static loads for the seismic design of long-span domes. These are determined from the maximum seismic accelerations, which may also be of use when designing the acceleration-sensitive non-structural components. The effect of post-yield stiffness of multi-storey substructure is studied by considering two structural systems incorporating buckling-restrained braced frames (BRBF) and spine frames. By using response spectrum analysis (RSA) and equivalent linearisation techniques, the maximum acceleration distributions in the horizontal and vertical directions are expressed using amplification factors by taking the effects of higher modes into account. These distributions are then used to obtain the equivalent static loads for design.

In addition, the effects of 2-Segmented spine frames as a response control strategy to suppress higher mode effects are also investigated. The design procedure is validated by comparing the results against those obtained from non-linear response history analysis (NLRHA).

2. RESPONSE CHARACTERISTICS OF LONG-SPAN DOME

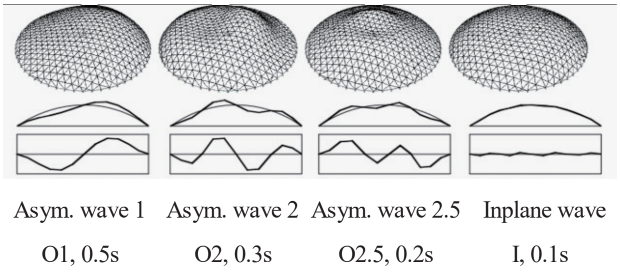

Figure 1: *Four principal modes: Periods and mode shapes of the dome*

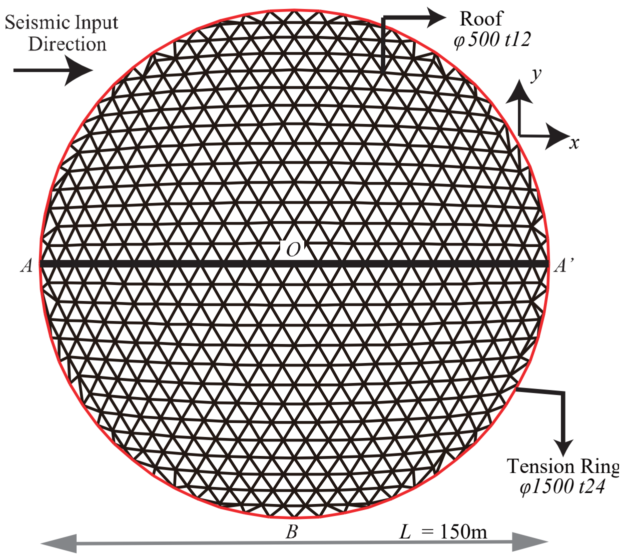

Figure 2: *Ridgeline shown in the plan view*

Studies conducted by Takeuchi et al. [7] in the past have indicated that double-layered domes exhibit vibration modes that are less varied than the single-layered ones. It was found that for depth-to-span ratios (of the double-layered domes) of 1/50 or more, the response characteristics become simpler and can be explained using the 4 prominent modes which are denoted as O1, O2, O2.5 and I (Figure 1).

In this study, the roof was modelled as a single-layered dome with a 150m span, and 30° half subtended angle (Figure 2).

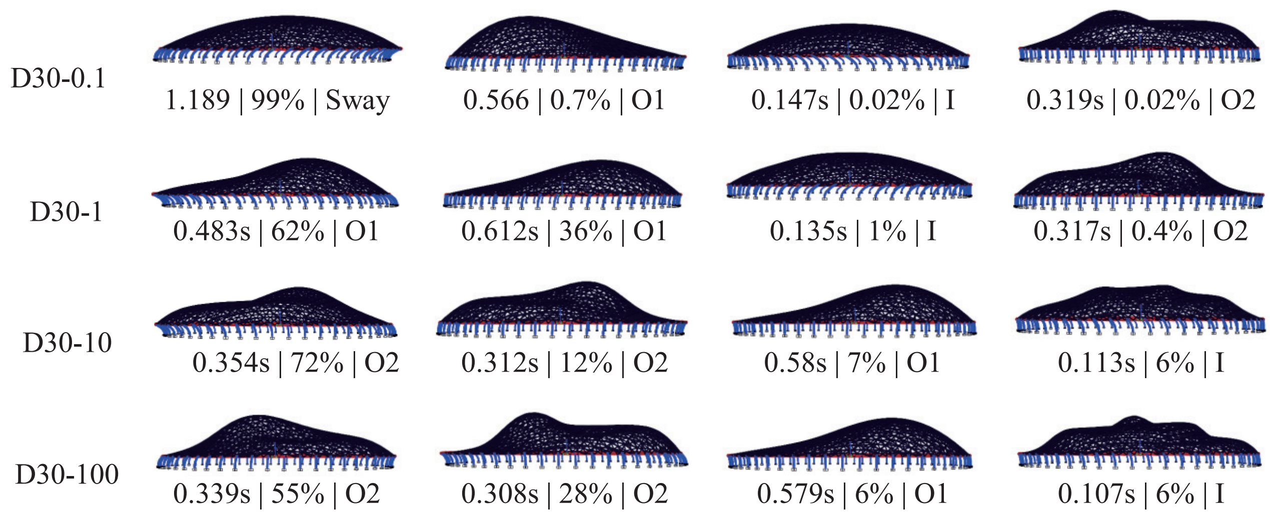

Figure 3: *Major vibration modes: Periods & mass participation factors along the x-direction*

The out of plane stiffness of the roof members was increased by a factor of 65 to model an equivalent double-layered dome of a depth-to-span ratio of 1/50. The dome consists of rigidly jointed circular hollow sections and was designed for a uniform 3 kPa dead load which includes an allowance for acoustic panels.

2.1. Effect of Substructure Stiffness

First, the dynamic characteristics of the dome are investigated using a simple supporting substructure that consists of single-storey columns pinned at the base (Table 1). A tension ring was modelled at the boundary of the dome. The connections between the tension ring and both substructure and roof are assumed pinned. The models are named as D30-α where α is the substructure stiffness amplification factor.

The major vibration modes of the roof mainly consist of the three principal mode shapes: O1, O2, and I (Figure 3). As the substructure stiffness increases, the mode with the highest mass participation factor gradually shifts from O1 to O2. When the substructure is very stiff, the roof has many closely spaced participating modes, with major vibration modes contributing to less than 80% of the mass participation. In most of the cases, the O2 mode seems to dominate and the contribution from the O2.5 mode is almost negligible. When compared with the prominent vibration modes of a medium-span dome [2], the periods of these modes are longer (Figure 4), as seen by mapping these modes on the target design acceleration spectrum [8]. In the case of domes with stiff substructure, all the prominent modes lie on the constant acceleration (maximum acceleration) region. In comparison, all but the O1 mode lie on the region with lower acceleration in the medium-span case (Figure 4). This implies that the magnitude of roof excitation of long-span roofs may be up to two times greater than the medium-span case, with greater contribution from the higher modes. Therefore, it is important to include these differences when estimating the peak design accelerations of long-span roofs.

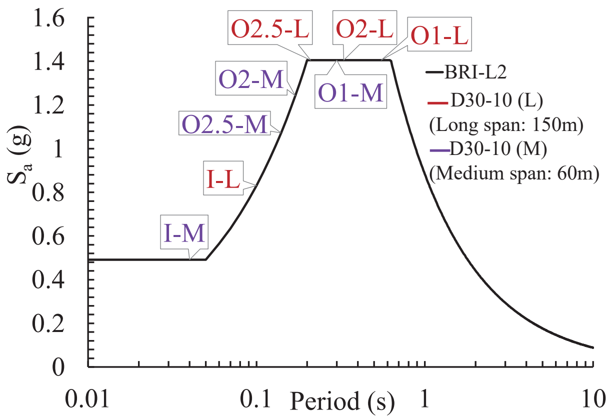

Figure 4: *Prominent mode shapes mapped on the target design spectrum (BRI-L2)*

3. EFFECTS OF MULTI-STOREY SUBSTRUCTURE

The analysis models used in this study are representative of large scale indoor stadiums or concert halls with seating capacities of about 20,000 people, which are being increasingly realised. 3-D ETABS [9] models were constructed and SN490 steel was adopted for all frame and roof members.

The frame sections and mass distribution for all of the models are summarised in Tables 1 and 2.

Table 1: *Frame sections data*

Member	Section	Size (mm)
Roof	CHS	$\phi 500\ t12$
Tension Ring	CHS	$\phi 1500\ t24$
MF Column	SHS	600×600×25
MF Beam	I	588×300×12×20
RF Brace	I	600×600×19×19

Table 2: *Model mass distribution*

Storey	Elevation (m)	Storey Weight (kN)
RFL	32	54018
6FL	21	18304
5FL	17.5	28507
4FL	14	28507
3FL	10.5	41121
2FL	7	41121
M2FL	3.5	41121

3.1. Types of Substructures

In this study, two types of supporting substructures are considered. The first type of substructure (Sub-BRB-MF) consists of a moment resisting frame (MRF) enveloping 16 pairs of braced frames, spaced equidistantly around the perimeter (Figure 5(a)). These braced frames employ energy-dissipating braces called buckling-restrained braces (BRBs) [10] arranged in a v-configuration. The substructure was designed using seismic design shear forces and *Ai* distribution defined in the Japanese code [8]. The design base shear force was calculated using a peak ground acceleration of 0.97g under a level-2 earthquake, keeping the moment frame elastic. This type of braced substructure is widely used to design buildings in countries of high seismic hazard, such as Japan and U.S.A.

The axial force-displacement of BRBs were determined assuming a post-yield stiffness ratio of 2% and parameters like total length (L_t), axial force (N_y), effective stiffness (k_{eff}), core-to-elastic area ratio (Ac/Ae) and plastic-to-work point length ratio (L_p / L_0) as shown in Table 3 following the design guidelines by Takeuchi and Wada [10].

The second substructure considered (Sub-Spine-MF) consists of damped spine frames in place of the braced frames (Figures 5(b) and 5(c)). The spine

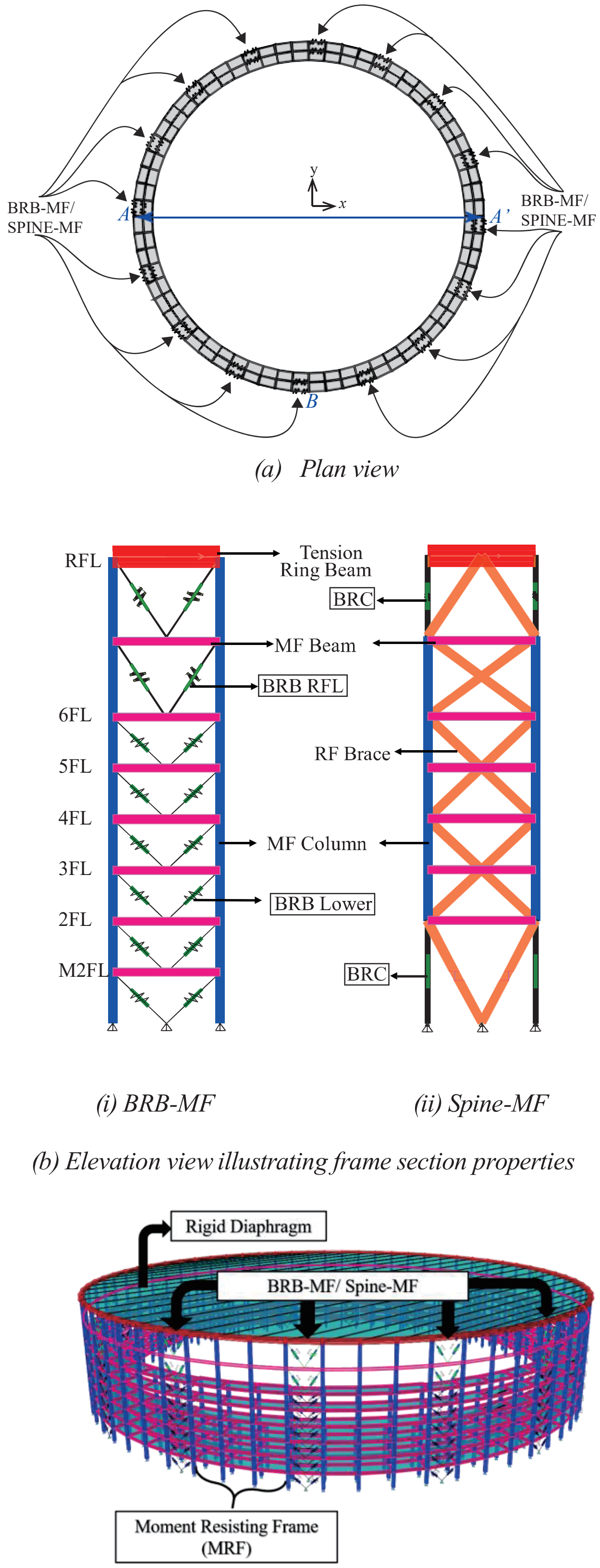

(a) Plan view

(i) BRB-MF *(ii) Spine-MF*

(b) Elevation view illustrating frame section properties

(c) 3-D view

Figure 5: *Substructure models*

frame utilises a stiff elastic braced steel frame with replaceable energy-dissipating members inserted vertically at the base (here, the BRBs are referred to as buckling restrained columns (BRC)). The spine frame prevents damage concentration at any particular storey while the enveloping MRF provides self-centring force and reduces residual drifts [11]. This substructure was designed to have the same initial stiffness and yield deformation as the equivalent Sub-BRB-MF. In both the models, the floors are assumed to be rigid and a rigid diaphragm was assigned to the roof.

***Table 3:** Specifications for BRBs in substructure*

Name	N_y (kN)	L_t (m)	k_{eff} (kN/m)	Material	A_c/A_e	L_p/L_0
BRC	3000	6	685285	LYP225	0.5	0.4
BRC	3000	7	685285	LYP225	0.4	0.3
BRB-RFL	1200	7	233578	LY225	0.5	0.3
BRB-Lower	1500	5	380587	LY225	0.5	0.3

The first two vibration modes (in order of decreasing mass participation factors β_i (%)) of the substructure models are given in Table 4 and the mode shapes are shown in Figure 6. The first mode of both substructures is a translational sway mode and this has a mass participation factor of less than 80%.

***Table 4:** Periods of the substructure models*

Model Name	Mode	T_i (s)	β_i (%)
Sub-BRB-MF	1	0.91	55
	2	0.39	35
Sub-Spine-MF	1	0.91	67
	2	0.30	25

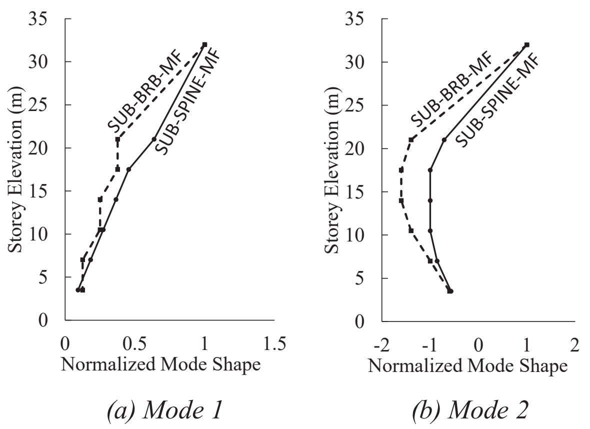

***Figure 6:** Mode shapes of substructures*

3.2. Response of Substructure

NLRHA was performed for the substructure models to study the seismic behaviour of the substructures (Figure 5). The input earthquake ground motion (El-Centro) was spectrally matched to the target design spectrum (BRI-L2) corresponding to a Level-2 earthquake as per the Japanese building code [8]. Equation (1) defines the design acceleration (S_a (cm/s^2)) where D_h is the reduction factor to adjust the damping ratio from the base damping ratio h_b=5%. The spectrum was adjusted to an inherent damping ratio h_o=2% using Equation (2) (Figure 7) [12].

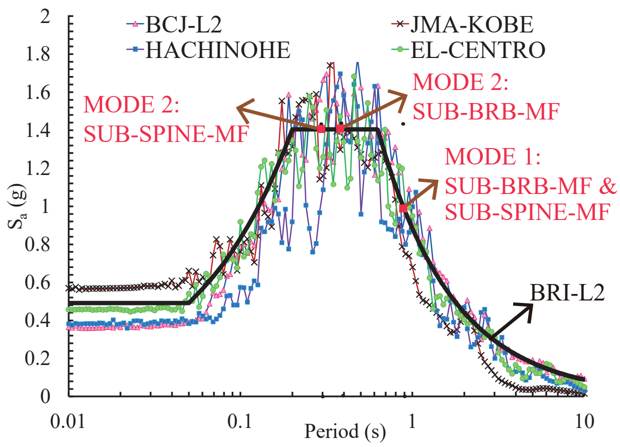

***Figure 7:** Design acceleration spectrum for level-2 earthquake (h_o=0.02)*

$$S_a(T) = \begin{Bmatrix} 350D_h & (T \le 0.05) \\ 350D_h(T/0.05)^{(1+\log(5/7)/\log 4)} & (0.05 < T \le 0.2) \\ 1000D_h & (0.2 < T < \pi/5) \\ 1000D_h/(T/2\pi) & (\pi/5 \le T) \end{Bmatrix} \quad (1)$$

$$D_h = \sqrt{(1+75h_b)/(1+75h_o)} \quad (2)$$

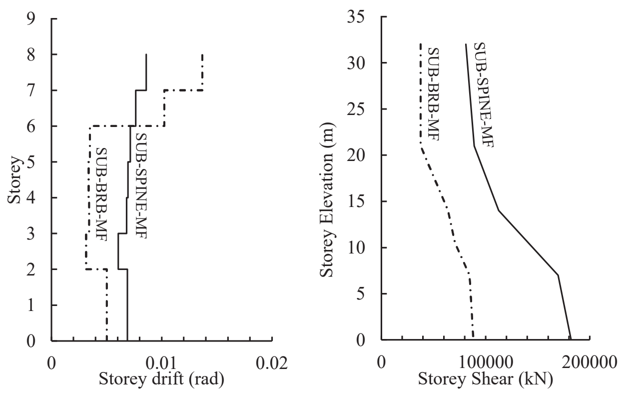

***Figure 8:** Maximum storey drift and shear force distributions for substructure models*

The storey drift and the shear force distribution for the two models are shown in Figure 8. The Sub-Spine-MF model exhibits a near-uniform storey drift distribution while the Sub-BRB-MF model tends to concentrate damage at the top storey (Figure 8). In contrast, the stiff spine frames effectively engage the neighbouring MRF to produce an even storey drift distribution. The larger shear forces in the Sub-Spine-MF model are a result of a higher post-yield stiffness (discussed in the later sections).

4. MODAL ANALYSIS OF COMBINED MODELS

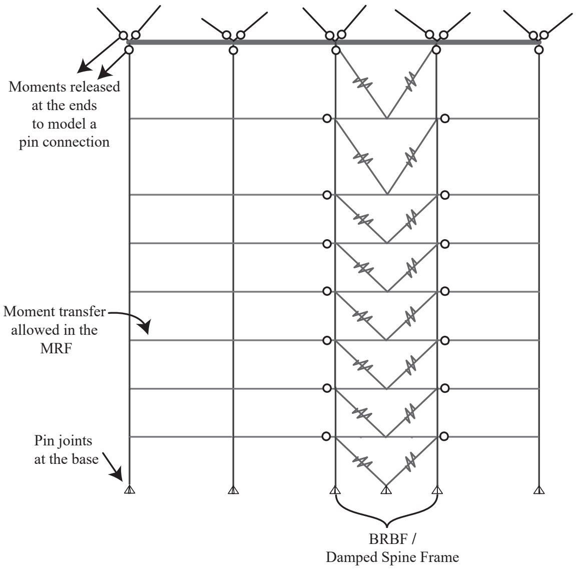

Figure 9: *Boundary conditions in combined models*

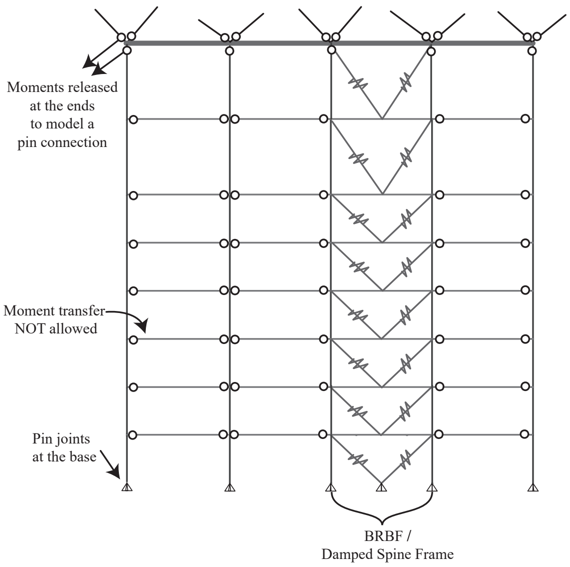

Figure 10: *Boundary conditions in combined pinned models*

The effects of a multi-storey substructure on the roof response are analysed by adding the dome roof model (Section 2) to the multi-storey substructure models (Section 3). The combined models are denoted as Spine-MF and BRB-MF (Figure 9). These models feature moment resisting frames (MRF) outside of the braced bays, with moment connections provided at the beams ends, but not at the column bases. Two additional models with pinned beam-column connections (Figure 10) are also included (Spine-P and BRB-P) in order to investigate the response of substructures with low post-yield stiffness.

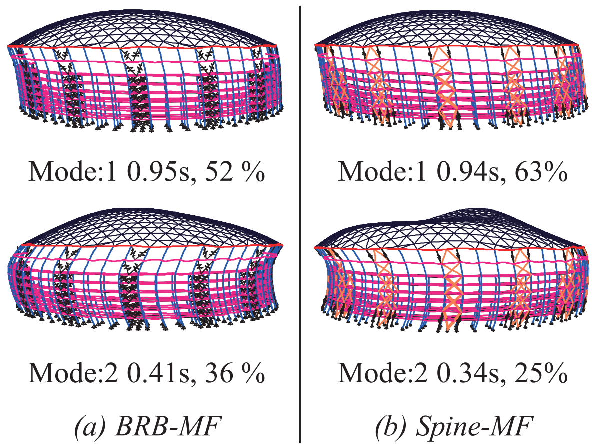

Figure 11: *Two dominant modes of combined models*

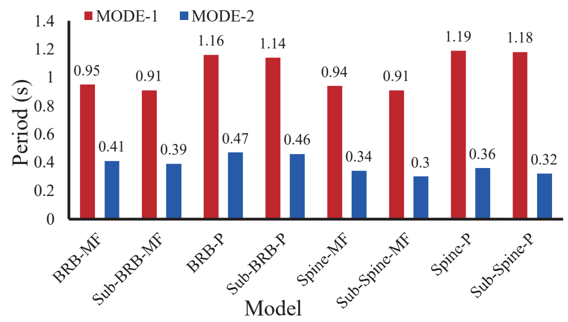

(a) Periods of two dominant modes

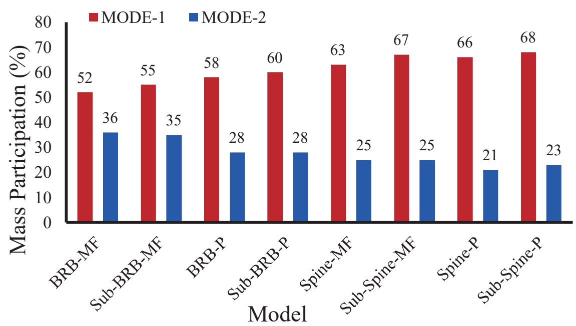

(b) Mass participation of two dominant modes

Figure 12: *Modal analysis results*

The first two dominant mode shapes of Spine-MF and BRB-MF are shown in Figure 11 and the modal analysis results of all the four combined and substructure models are summarised in Figure 12. The periods of the first two modes are very close to the corresponding periods of their substructure models and the mass participation factors are nearly equal. For the combined models shown in Figure 11, the first mode is essentially a combination of the translational sway mode of the substructure and the roof's O1 mode. The second mode of the two models is slightly different. This is because Spine-MF is slightly stiffer than BRB-MF in the second mode.

The substructure in both the models vibrates in its respective (translational) second mode. In the second mode of Spine-MF model, the O2 roof mode (highermode) is excited as the period 0.34s coincides with the roof's O2 mode (Section 2). For the BRB-MF case, the second mode lies between the O2 and the O1 mode of the roof, but since it is closer to the O1 mode, the roof appears to vibrate in its O1 mode. As opposed to the medium-span domes, the first mode of the long-span domes generally lies on the constant-velocity region of the design acceleration spectrum while the second mode lies on the constant acceleration region of the design spectrum as shown in Figure 7. This implies a greater contribution of the higher modes to the overall response.

5. PROCEDURE TO OBTAIN EQUIVALENT STATIC LOADS

While significant advances have been made over the past decade, seismic design codes and manuals fail to provide quantitative guidance on the seismic design of long-span domes. Furthermore, higher mode effects on seismic response control of long-span domes with yielding multi-storey substructures have not been captured yet. Hence, a design procedure to estimate the equivalent static loads of long-span domes considering the plasticity of substructure and incorporating the higher mode effects is proposed (Figure 13).

Step 1 Obtain the substructure periods.

From the eigenvalue analysis, obtain the periods of the substructure model (T_i) corresponding to n dominant modes with a combined mass participation factor of at least 90% ($\sum\beta_i > 90\%$).

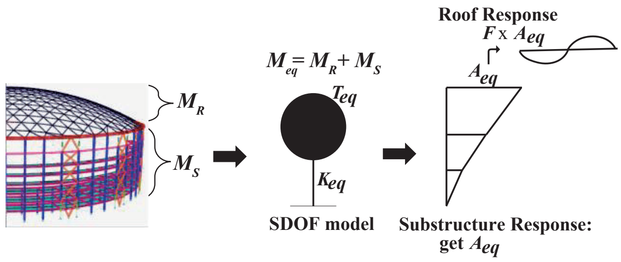

Figure 13: *Simplified illustration of the procedure to obtain roof response*

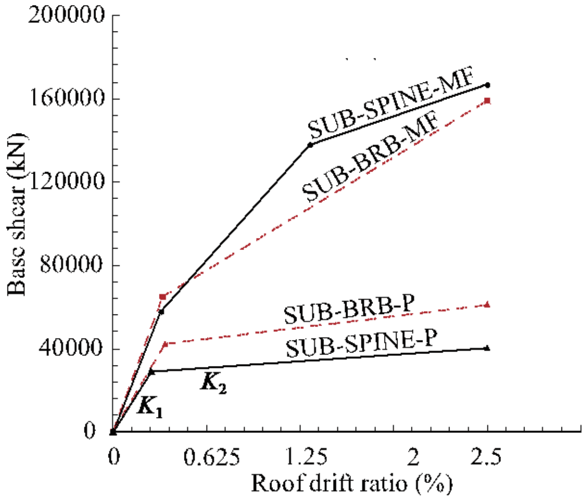

Figure 14: *Simplified first modal pushover curve for the substructure models*

Step 2 Perform modal pushover analysis of the substructure.

Perform nonlinear pushover analysis (derived from the fundamental mode shape) on the global substructure model (with the roof as a rigid diaphragm and mass), permitting the moment frame beam ends and BRBs to yield. Note that only a pushover curve of the base shear by roof displacement is required for the subsequent analysis.

From the modified modal pushover methodology proposed by Chopra et al. [13], the higher mode response of the substructure estimated using the elastic modes gives a conservative estimate of the seismic demand, while reducing the computational effort. An equivalent approach is adopted in this paper, where the higher mode contribution is obtained using the initial elastic stiffness (K_{1i}) for mode i.

In this study, to simplify the behaviour, the first-mode curves were bi-linearised by matching the areas at 2.5% roof drift (Figure 14). The Sub-Spine-MF is better simplified as a tri-linearised curve to mark the two distinct yield points which correspond to yielding of the spine frame and yielding of the moment frame beams [11]. However, for this study, it was observed that the beams did not yield in the level-2 earthquake. Calculate the ratio of the post-yield stiffness to the elastic stiffness (K_{2i} / K_{1i}) for all the models from the bi-linearised curves. The initial stiffness in the first (K_{11}) and second mode (K_{12}) are listed in Table 5.

Table 5: *Base Shear vs Roof Displacement: stiffness in each mode (kN/mm)*

Model	K_{11}	K_{11} / K_{21}	K_{12}	K_{12} / K_{22}
BRB-MF	615	4.5	4600	1
Spine-MF	562	2.2	5896	1
BRB-P	381	15	2820	1
Spine-P	354	22	4160	1

Figure 15 shows the deformed shape of the substructures at the end of the first modal pushover analysis at 2.5% roof drift. The model employing spine frames deforms uniformly along the storey height. The beams of the moment frame yield evenly, implying that damage is not concentrated at any particular storey. However, the BRB-MF deformations are less uniform. The deformation at the top storey is much larger than the bottom storeys.

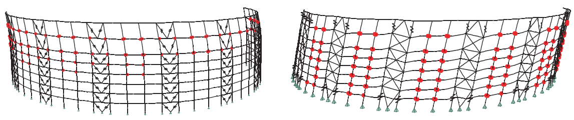

(a) Sub-BRB-MF *(b) Sub-Spine-MF*

Figure 15: *Elevation A-B-A': Deformed shape after pushover (dots mark the yielded beams)*

Step 3 Obtain the peak elastic roof acceleration of the substructure.

For each mode, use the elastic design acceleration spectrum to obtain the base shear and then extrapolate the maximum elastic roof displacement from the initial stiffness of the pushover curve (K_{1i}). The maximum roof acceleration A_i of the substructure is obtained from the corresponding roof displacement and period for each mode.

Step 4 Obtain the equivalent damping ratio and reduction factor.

The equivalent stiffness (K_{eqi}) and equivalent damping ratio (h_{eqi}) are obtained using the equivalent linearisation procedure proposed by Kasai et al. [12], which estimates the peak response of elasto-plastic systems. For each of the modes, assume a starting value of ductility ratio μ_i and iterate h_{eqi} and K_{eqi} / K_{1i} using Equations (3)-(6) until μ_i converges, where the subscript (j) is the jth step of the iteration. In case of Spine-MF models where the peak roof drift falls in the third region of the pushover curve, K_{eqi} can be calculated using the equivalent linearisation procedure given by Chen et al. [11].

$$K_{eqi} / K_{1i} = 1/\mu_i + (1 - 1/\mu_i) K_{2i} / K_{1i} \tag{3}$$

$$h_{eqi} = h_{oi} + \frac{2(K_{1i} / K_{2i})}{\pi \mu_i} \ln \frac{K_{1i} / K_{2i} + \mu_i - 1}{(K_{1i} / K_{2i}) \mu_i^{K_{2i}/K_{1i}}} \tag{4}$$

$$D_{hi} = \sqrt{(1 + 25 h_{oi}) / (1 + 25 h_{eqi})} \tag{5}$$

$$\mu_{i(j)} = \mu_{i(1)} D_{hi(j-1)} / \sqrt{K_{eqi(j-1)} / K_{1i}} \tag{6}$$

Step 5 Calculate the equivalent periods and inelastic peak roof accelerations of the substructure.

For each of the modes, calculate the equivalent (secant) period T_{eqi} and the peak accelerations A_{Heqi} and A_{Veqi} of the SDOF model using Equations (7)-(11). A_{Heqi} and A_{Veqi} are the peak inelastic accelerations of the SDOF model.

$$T_{eqi} = T_i \sqrt{K_{1i} / K_{eqi}} \tag{7}$$

1. For modes with T (s) and T_{eq} (s) in the constant acceleration region:

$$A_{Heqi} = A_i D_{hi} \tag{8}$$

$$A_{Veqi} = A_i \tag{9}$$

2. For modes with T (s) and T_{eq} (s) in the constant velocity region:

$$A_{Heqi} = A_i D_{hi}\sqrt{K_{eqi} / K_{1i}} \quad (10)$$

$$A_{Veqi} = A_i\sqrt{K_{eqi} / K_{1i}} \quad (11)$$

Step 6 Calculate the roof amplification factors.

After obtaining the peak response of the substructure, the next step is to calculate the horizontal and vertical amplification factors. Takeuchi et al. [2] demonstrated that the seismic roof response can be evaluated in a simple manner using amplification factors, derived from the response characteristics of a simple lumped mass arch model. The present study applies the same fundamental concepts to long-span domes.

Previously, the amplification factors were proposed to obtain the overall roof response including minor contributions from the higher modes (O2, O2.5 and I) of the roof, but these were calculated based on the period ratio obtained only from the first mode of the substructure [2]. This study extends the previous proposal to include contributions from other higher substructure modes. Use Equations 12 and 13 to estimate the amplification factors F_{Hi} and F_{Vi} for the horizontal and vertical directions. θ is the half subtended angle; $R_{Ti} = T_{eqi} / T_R$ is the ratio of the equivalent period of the SDOF model to that of the roof O1 mode; $R_M = M_{eq} / M_R$ is the ratio of SDOF model to roof mass; and the calibration factor C_V is taken as 1.88 [2].

$$F_{Hi} = \begin{cases} 3 & (0 < R_{Ti} \le 5/36) \\ \sqrt{5/4R_{Ti}} & (5/36 < R_{Ti} \le 5/4) \\ 1 & (5/4 < R_{Ti}) \end{cases} \quad (12)$$

$$F_{Vi} = \begin{cases} 3C_V\theta & (0 < R_{Ti} \le 5/16) \\ (\sqrt{5/R_{Ti}} - 1)C_V\theta & (5/16 < R_{Ti} \le 5) \\ 0 & (5 < R_{Ti}) \end{cases} \quad (13)$$

Step 7 Calculate modified amplification factors to consider harmonic resonance.

When $R_M > 2$ and $R_T \sim 1$, harmonic resonance must be taken into account [14]. Harmonic excitation of the roof is expected to occur when the O1 mode of the roof coincides with the substructure period and the substructure is much heavier than the roof. In such cases, the modified amplification factors $F_H{}'$ and $F_V{}'$ for the equivalent period (T_{eqi}) are calculated using Equations (14) and (15).

$$F'_{Hi} = \sqrt{F_{Hi}{}^2 + \frac{1}{(1 - R_{Ti}{}^2)^2 + (1/R_M)^\theta}} \quad (14)$$

$$F'_{Vi} = \sqrt{F_{Vi}{}^2 + \frac{1}{(1 - R_{Ti}{}^2)^2 + (1/R_M)}} \quad (15)$$

Step 8 Obtain the peak roof acceleration distributions.

Compute the acceleration distributions A_{Hi} and A_{Vi} using the calculated amplification factors; where x and y are the coordinates of roof nodes with $\{x, y\} = \{0,0\}$ as the centre and L is the span of the dome (Equations (16) – (18)).

1. Horizontal acceleration distribution

Since the horizontal acceleration is not particularly sensitive to the dominant mode shapes, Equation (16) is sufficient to capture the response in the horizontal direction.

$$A_{Hi}(x, y) = A_{Heqi}\{1 + (F_{Hi} - 1)\cos\frac{\pi\sqrt{x^2 + y^2}}{L}\} \quad (16)$$

2. Vertical acceleration distribution

As discussed in Section 2, the vertical acceleration distribution is sensitive to the shape of the contributing modes. Previously, the equation for vertical acceleration distribution was formulated exclusively based on the O1 mode [2]. Here, it is proposed to adopt a weighted acceleration distribution that includes contributions from the O2 and O2.5 mode shapes, as required (Figure 1). Since the higher excited modes in this study are predominantly O1 and O2 modes, the distribution is extended to the O2 mode, as proposed in Equation (18).

The distribution of the vertical acceleration should be selected according to the excited roof mode. For example, if a certain mode of the structure exhibits the roof in O1 mode, then the vertical acceleration contribution for that mode should be determined from Equation (17). Similarly, if the mode consists solely of the translational sway of the substructure, A_{Vi} may be taken as zero.

- O1 mode:

$$A_{Vi}(x,y) = A_{Veqi} F_{Vi} \frac{x}{\sqrt{x^2+y^2}} \sin \frac{2\pi\sqrt{x^2+y^2}}{L} \quad (17)$$

- O2 mode:

$$A_{Vi}(x,y) = \begin{cases} d & (|x| \le L/4) \\ 0.5d & (|x| > L/4) \end{cases} \quad (18)$$

where $d = A_{Veqi} F_{Vi} \frac{x}{\sqrt{x^2+y^2}} \sin \frac{2\pi\sqrt{(2x)^2+(2y)^2}}{L}$

Step 9 Compute the combined roof accelerations.

Combine the modal accelerations at each node using Equations (19) and (20) to obtain the envelope. This study uses the absolute summation rule. Similarly, the peak displacements can also be obtained.

$$A_H(x,y) = \sum_{i=1}^{n} |\beta_i A_{Hi}(x,y)| \quad (19)$$

$$A_V(x,y) = \sum_{i=1}^{n} |\beta_i A_{Vi}(x,y)| \quad (20)$$

Step 10 Calculate the equivalent static loads.

Finally, evaluate the equivalent static seismic forces for each node from the nodal mass m_k and acceleration $A_H(x,y)$ or $A_V(x,y)$ at position (x,y) using Equations (21) and (22).

$$f_H(x,y) = m_k A_H(x,y) \quad (21)$$

$$f_V(x,y) = m_k A_V(x,y) \quad (22)$$

Conduct static pushover analysis by applying the vertical and horizontal loads simultaneously to the roof nodes in each of the patterns as shown in Figure 16. Adopt the maximum response (axial force and bending moment) in each member from the four static load cases as the preliminary seismic demand.

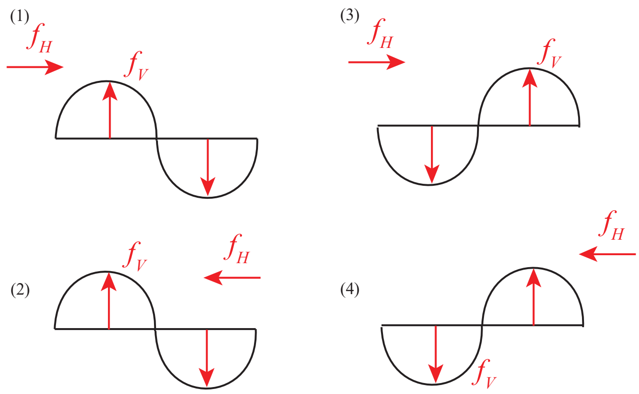

Figure 16: *Static Load Patterns*

6. ACCURACY OF THE PROPOSED METHOD

NLRHA was performed on all the four models (Figure 12) to validate the proposed design procedure permitting the beams in MRF, BRCs and BRBs to yield. The beams in MRF are assumed to have sufficient lateral support. The proposed design procedure was applied using the first two dominant modes (Figure 12). Four input ground motions (El-Centro, Hachinohe, BCJ-L2 and JMA-Kobe) were used, each was spectrally matched to the BRI-L2 design spectrum (Figure 7). 2% Rayleigh damping was applied to the first two dominant modes. It should be noted that geometric non-linearity, P-delta secondary effects and wave-passage effects are not included in this study for simplicity. The acceleration distributions along the ridgeline A-O-A' are shown in Figure 17, and the maximum axial forces and bending moments obtained from the static load cases are compared with the NLRHA results in Figure 18. The main parameters are summarised in Table 6.

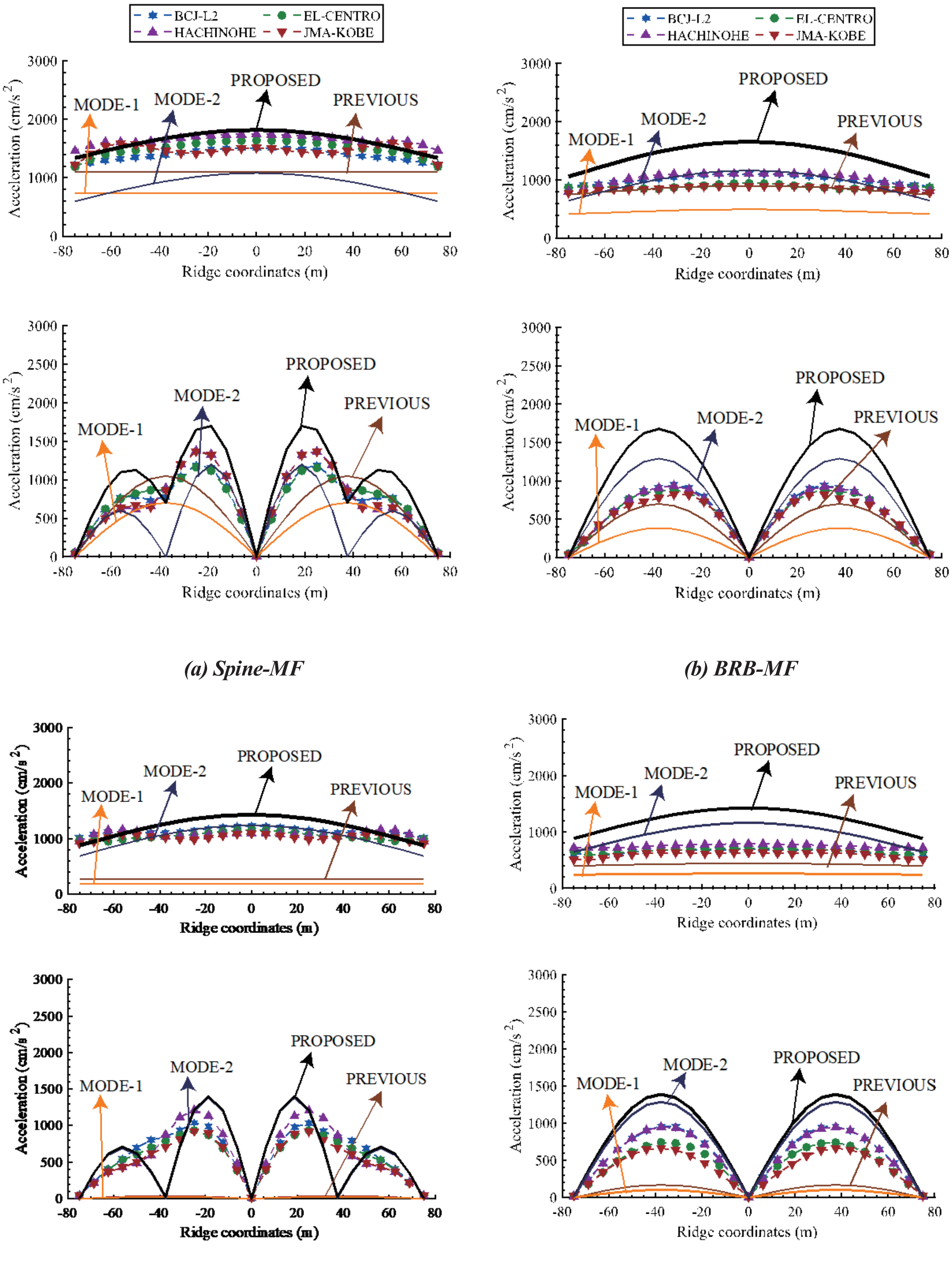

(a) Spine-MF *(b) BRB-MF*

(c) Spine-P *(d) BRB-P*

Figure 17: *Inelastic response: Horizontal acceleration (top) and Vertical acceleration (bottom)*

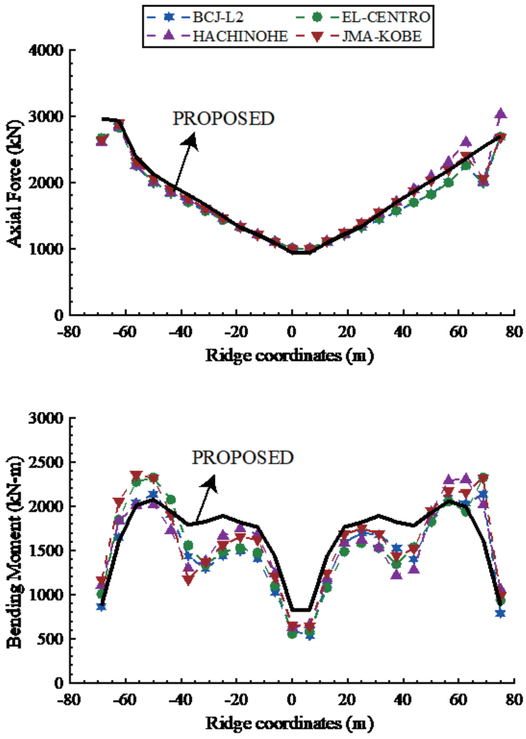

(a) Spine-MF

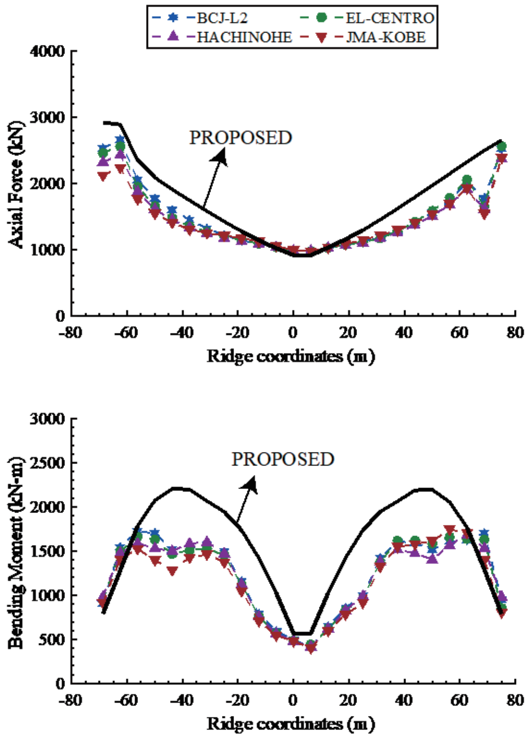

(b) BRB-MF

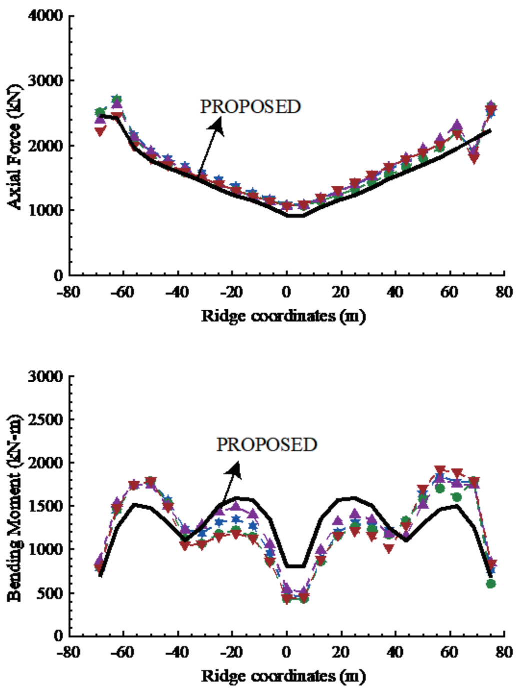

(c) Spine-P

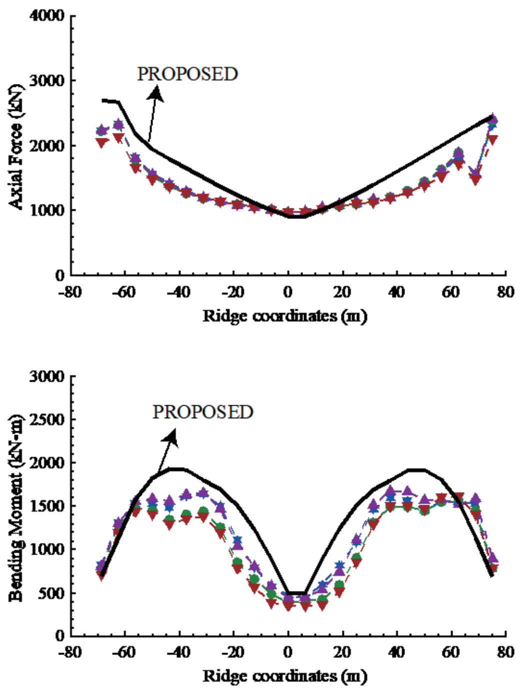

(d) BRB-P

Figure 18: *Axial Forces (top) and Bending moments (bottom)*

The combined acceleration response obtained using the proposed method (Section 5) is labelled as 'PROPOSED' while the modal contributions ($|\beta_i A_{Hi}(x,y)|$ or $|\beta_i A_{Vi}(x,y)|$) of the first and second modes are labelled as 'MODE-1' and 'MODE-2'. The response calculated according to Takeuchi et al. [15], which only considers the first mode of the substructure (with β_1 equal to 100%), is labelled as 'PREVIOUS'. The acceleration distributions throughout the dome for Spine-MF are shown in Figures 19 and 20. A similar correlation was observed for the other models. The results are in good agreement with the results obtained from NLRHA.

***Table 6:** Main Parameters: Proposed method*

Mode	β (%)	T (s)	D_h	K_{eq}/K_1	μ	Teq (s)	A_{Heq} (cm/s^2)	A_{Veq} (cm/s^2)
(i) BRB-MF								
1	55	0.91	0.57	0.47	3.14	1.33	750	1300
2	35	0.39	1.00	1.00	1.00	0.39	1900	1900
(ii) Spine-MF								
1	67	0.91	0.68	0.64	3.61	1.13	1100	1600
2	25	0.30	1.00	1.00	1.00	0.31	2400	2400
(iii) BRB-P								
1	60	1.14	0.48	0.31	3.91	2.05	400	860
2	28	0.46	1.00	1.00	1.00	0.45	2300	2300
(iv) Spine-P								
1	68	1.18	0.41	0.20	5.98	2.61	280	700
2	23	0.32	1.00	1.00	1.00	0.32	3000	3000

The excitation of the O2 mode in the Spine-MF model is evident from the dual peaks appearing in the distribution of vertical acceleration. In comparison to the Spine-MF model, the first modal response in the case of BRB-MF model is less pronounced due to the lower first mode mass participation factor of the substructure (Table 4). The results for BRB-P and Spine-P shown in Figure 17 confirm that only considering the first mode for response underestimates the peak accelerations. Including the predominant higher modes significantly improves the accuracy of response estimation.

The substructure yields for all the models in the first mode, significantly reducing the first mode contribution to the overall response, evident from the reduced A_{Heq1} and A_{Veq1} values. A reduction of about 40-50% was observed for the horizontal accelerations and about 20-30% for the vertical accelerations. The reduction was more in the BRB-MF model as compared to the Spine-MF model due to the lower post-yield stiffness of the substructure (i.e. lower K_{21}/K_{11} value). The reductions in vertical acceleration values due to the added dampers are found to be lesser than those in the horizontal accelerations. Similar observations were made by Takamatsu et al. [16] while studying seismically isolated domes where the reductions in vertical acceleration were primarily due to the elongated period. Hence, in this study, the effect of additional damping was neglected while estimating the vertical response (Equations (9) and (11)).

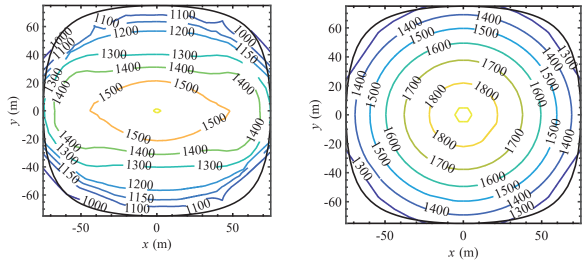

(a) NLRHA *(b) Proposed*

***Figure 19:** Horizontal acceleration (cm/s^2): Spine-MF*

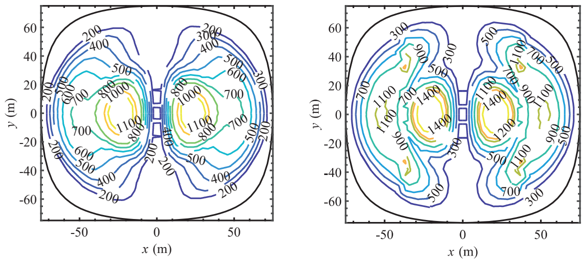

(a) NLRHA *(b) Proposed*

***Figure 20:** Vertical acceleration (cm/s^2): Spine-MF*

In the case of the simply-supported BRB-P and Spine-P models (Figure 17), the contribution of the first mode to the overall response is negligible compared to the second mode. This is because the post-yield stiffness of the substructure is negligible as evident from the near elastic-perfectly-plastic pushover curve (Figure 14). This results in longer equivalent periods (T_{eq1}) and larger response reductions ($D_h \sim 0.5$) explaining the low values of peak accelerations. However, the substructure is still elastic in the second mode, which implies that T_{eq2} for these models still lies in the maximum acceleration region of the response spectrum which results in such high A_{Heq2} and A_{Veq2} values. This also suggests that there is a need to introduce response control strategies that can effectively reduce the response not only of the first mode but also of the significant higher modes.

The maximum axial forces and bending moments obtained from NLRHA are also compared with those obtained from the proposed equivalent static loads as shown in Figure 18. The axial forces are in good agreement with the maximum response values, and the response variation between the four input ground motions is negligible. The maximum bending moments have greater variation as the envelope is sensitive to the specific roof modes that are excited. Takeuchi et al. [14] also observed this phenomenon in a study of medium-span domes supported by elastic multi-storey substructures. The proposed values provide a good approximation of the trends, and so are useful for preliminary design, but final check using a more advanced NLRHA analysis and minor changes to member sizes may be required.

7. EFFECTS OF 2-SEGMENTED SPINE FRAME SYSTEMS

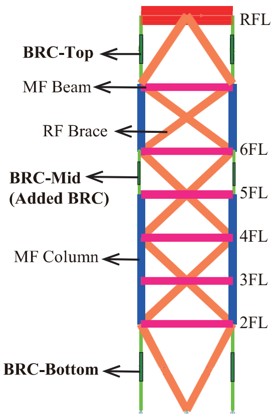

Figure 21: *2-Segmented spine frame: Location of BRCs*

Segmented spine systems were proposed by Chen et al. [17] to control the response of high-rise structures with significant mass participation from higher modes. These systems effectively reduced the response of high-rise buildings vis-a-vis the 1-Segmented spine system. Therefore, an additional 3-D model with substructure employing 2-Segmented spine frames (Figure 21) instead of the conventional 1-Segmented spine frame (previously the Spine-MF model) is studied and the effects of 2-Segmented spine frame on the roof response are investigated.

It was concluded by Chen et al. [17] that for an upper-to-lower damper stiffness ratio greater than 0.5, the response reduction effects are similar. Hence, for simplicity, the stiffness and material properties of the added BRCs (BRC-MID) were kept the same as the original BRC-Bottom (Table 7) resulting in a yield force that is half of the yield force of the BRC-Bottom. The frame section properties and mass distribution are also the same as that of the 1-Seg model (Tables 1 and 2).

Table 7: *Stiffness ratio of BRCs*

BRB Type	Stiffness Variable	Stiffness Ratio (K_M / K_B)
BRC-Top	K_B	1-Seg: N/A 2-Seg: 1
BRC-Middle	K_M	
BRC-Bottom	K_B	

7.1. Modal Analysis and NLRHA

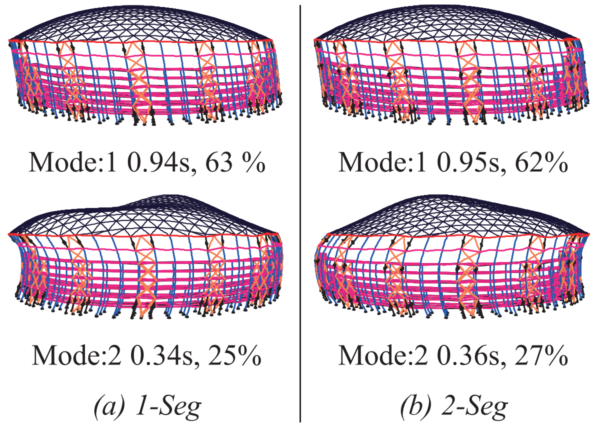

Figure 22: *Two dominant modes: Mode shapes*

The periods of the first two dominant modes of the 1-Seg Spine and 2-Seg Spine models are shown in Figure 22. The mode shapes of both the substructures are found to be nearly identical with a more even distribution observed for the 2-Seg model. The addition of a second spine frame caused a slight increase in the mass participation of the second mode while decreasing the mass participation of the first mode. For both the combined models, the first mode is a translational sway mode. The roof appears to vibrate in the O2 mode in the second mode of the models. However, the heights of troughs and crests observed in the roof of the 2-Seg model are relatively smaller.

Allowing the beams and BRCs to yield, NLRHA was performed on the 3-D models (Figure 22). The average peak accelerations for 2-Segmented spine models are lower than the 1-Segmented spine model

(Figure 23). The change in the shape of the vertical acceleration distribution from 1-Seg to 2-Seg spine model indicates a transition towards the predominance of the first mode (O1 mode) of the roof. This shows that implementing response control strategies for higher modes can be employed to suppress the higher mode effects to a certain extent.

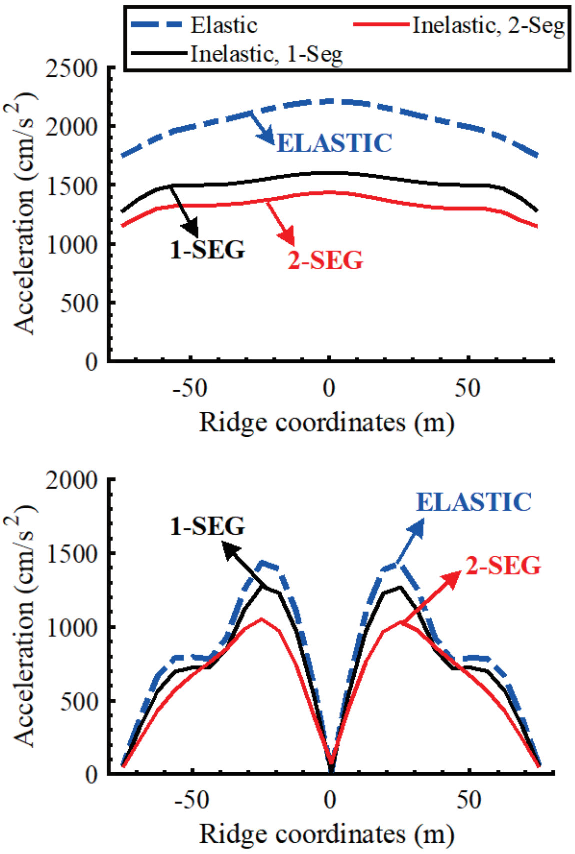

Figure 23: *Average Response of 2-Seg and 1-Seg: Horizontal (top) and Vertical (bottom) acceleration*

7.2. Equivalent Static Loads

The equivalent static loads for the dome of the 2-Seg model were obtained using the procedure as proposed in Section 5.

The first two modal pushover curves (first two dominant modes) of the substructure are shown in Figure 24. The maximum elastic roof acceleration A_i of the substructure was obtained from the corresponding roof displacement and period for each mode. As yielding is expected to occur in the second mode, the following modification was applied to include the post-yield response from the second mode of the substructure:

Modified Step 5: Consider acceleration reduction in the second mode of the substructure (previously, reduction in only the first mode response was considered and the ratio K_{22} / K_{12} was 1) according to the region of the design spectrum where the corresponding period lies (Equations (8)-(11)).

The first modal pushover curve is found to be similar to that of the 1-Seg Spine model with approximately the same yielding points and stiffness ratios. The second mode has a much larger initial as well as post-yield stiffness. However, a significant reduction was observed in the peak substructure response in the second mode with the reduction factor D_h being same in both the first and second modes. In addition, the energy dissipated by the added BRC (BRC-Mid) was around 10% of the input energy while the energy dissipated by the BRC-Bottom was around 40% of the input energy.

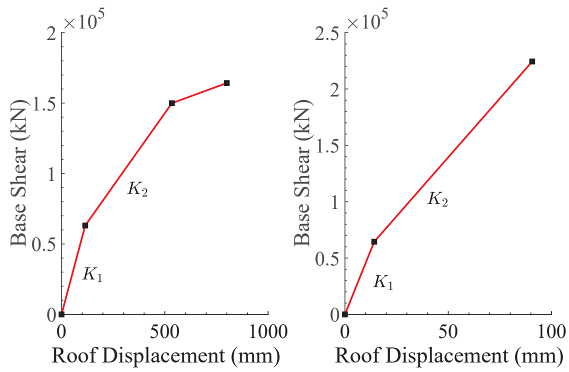

(a) 2-Seg, Mode 1 *(b) 2-Seg, Mode 2*

Figure 24: *Modal pushover curves of substructure*

The peak inelastic accelerations of the substructure were then used to obtain the horizontal and vertical acceleration distribution in the roof. The main parameters obtained for the 2-Seg model are summarised in Table 8 and the acceleration distribution along the ridgeline is shown in Figure 25(a). The proposed accelerations, although conservative in the vertical direction, are in good agreement with the NLRHA results. The added damping resulted in overall lower peak accelerations in the 2-Seg model.

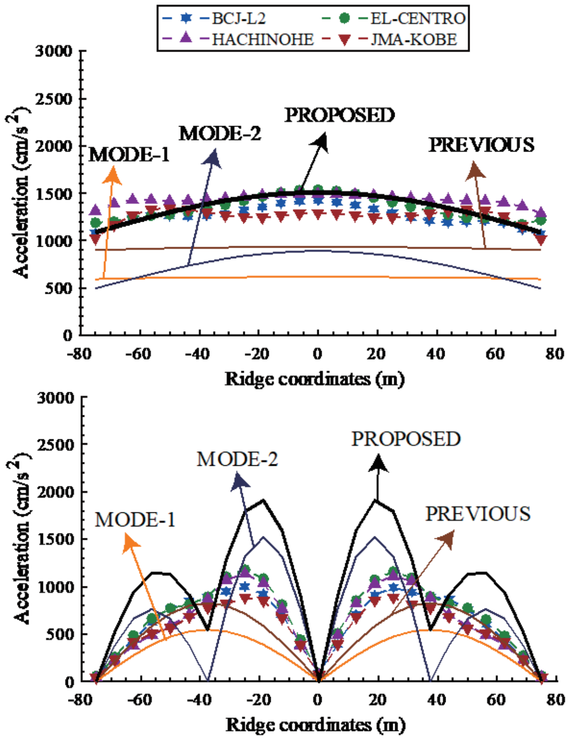

(a) Horizontal & Vertical Accelerations

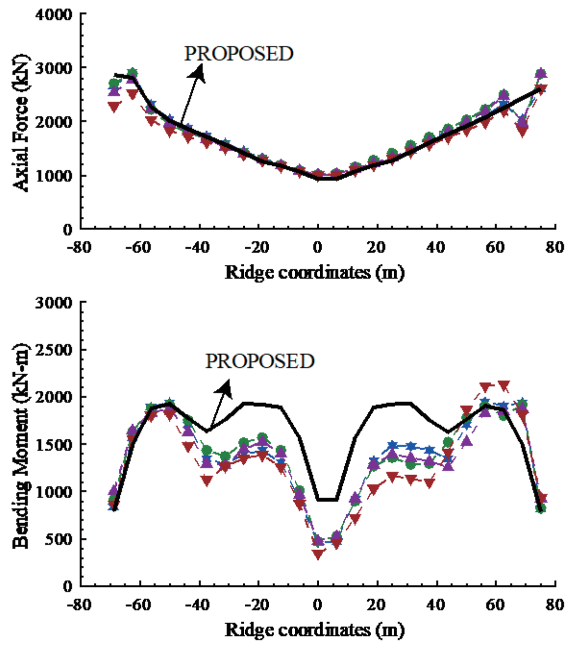

(b) Axial Forces & Bending Moments

Figure 25: *2-Seg combined model response*

Table 8: *Parameters of 2-Seg Model: Inelastic response*

Mode	β (%)	T (s)	D_h	K_{eq}/K_1	μ	Teq (s)	A_{Heq} (cm/s^2)	A_{Veq} (cm/s^2)
1	66	0.92	0.65	0.59	2.91	1.13	900	1400
2	26	0.32	0.65	0.57	4.75	0.43	1900	2900

The maximum axial forces and bending moments along the ridgeline obtained from the four equivalent static load cases (Figure 16) are also compared with the corresponding maximum results obtained from the NLRHA as shown in Figure 25(b). The axial forces are in good agreement with the NLRHA results, despite the slightly conservative accelerations. Similarly, the bending moments are on the conservative side, but with the error slightly asymmetric along the centreline. This may be because the moments are more sensitive to the slight irregularities in the mesh geometries near the boundaries of the domes and specific roof mode shapes. The axial forces and the bending moments in the 2-Seg spine model are less than the 1-Seg spine model due to the additional damping effect. Thus, the 2-Seg model generally performs better than the 1-Seg model and provides a good option for long-span domes, further improving the response of the 1-Seg spine substructure.

8. CONCLUSIONS

The seismic response characteristics of long-span domes with multi-storey substructures are investigated. Simple equations to evaluate the inelastic response and a procedure to estimate the equivalent static loads for preliminary design are proposed. The accuracy of the proposed method is also evaluated using NLRHA. From this investigation, the following conclusions are drawn:

1. The magnitude of roof excitation in long-span domes may be significant despite the elongated natural periods. For domes with higher modes lying on the constant acceleration region of the design spectrum, the contribution of higher modes with significant values of mass participation factor must be included when estimating the overall response of the dome.
2. It is important to consider higher modes when evaluating the response of long-span domes when the natural period of the asymmetrical mode is long and lies on the constant-velocity region of the design spectrum. For substructures lacking MRF, significant reduction in accelerations is expected when judged from the first modal response due to the near elastic-perfectly-plastic pushover curves. However, the higher modes are still in the elastic range and hence significantly contribute to the overall response, resulting in the large combined accelerations.

3. The proposed design procedure incorporates yielding of a multi-storey substructure using equivalent linearisation procedure. The responses estimated by this method are in good agreement with those obtained from NLRHA and this method is suitable for the preliminary design of such domes with multi-storey substructures.

4. The proposed method relies on modal pushovers using the first two dominant modes of the substructure to obtain the peak substructure response. For substructures that yield in higher modes, the modified procedure can be used that incorporates yielding in higher mode.

5. The distribution of the roof response may be different for two structures having similar periods and mass distribution, as the distribution of vertical acceleration is sensitive to the shape of the roof in the participating modes. It is proposed to adopt a weighted acceleration distribution that includes the contribution of the higher mode shapes and a new equation was formulated for the distribution of vertical acceleration in the higher mode.

6. Adding spine and braced frames in the substructure proved to be effective in reducing the roof response. However, this was limited to the response derived from the first mode. Incorporating a two-segmented spine frame system in the substructure was found to be an effective response control strategy to reduce the response due to the higher modes.

7. The proposed method provides an accurate estimate of the accelerations and axial forces across the dome. However, the bending moments are found to be sensitive to the excited roof modes and substructure characteristics. Further studies are required to accurately capture the bending moment distribution, but the present proposal provides a good approximation of the trends and is sufficiently accurate for preliminary design.

REFERENCES

[1] T. Ogawa, T. Takeuchi, M. Nakagawa, and T. Kumagai, "Seismic response analysis of single layer lattice domes," in *Proceedings of IASS-APCS 2003*, (Taipei, Taiwan), pp. 110–111, October 22-25 2003.

[2] T. Takeuchi, T. Ogawa, and T. Kumagai, "Seismic response evaluation of lattice shell roofs using amplification factors," *Journal of the IASS*, vol. 48, pp. 197–210, 2007.

[3] T. Kumagai, T. Takeuchi, T. Ogawa, A. Nakama, and E. Sato, "Seismic response evaluation of latticed domes with elasto-plastic substructures using amplification factors," in *Proceedings of IASS 2005*, (Bucharest, Romania), pp. 383–390, September 6-10 2005.

[4] S. Kato and S. Nakazawa, "Seismic design method to reduce the responses of single layer reticular domes by means of yielding of substructure under severe earthquake motions," in *Proceedings of IASS 2001*, (Nagoya, Japan), p. TP077, October 9 - 13 2001.

[5] S. Kato, Y. Konishi, and S. Nakazawa, "Pushover analysis and static estimation of seismic response of large steel space structures," *Proceedings of the IASS-APCS 2003*, pp. 54–55, 2003.

[6] S. Kato, S. Nakazawa, and K. Saito, "Two-mode based estimation of equivalent seismic loads and static estimation of dynamic response of reticular domes supported by ductile substructures," *Journal of the IASS*, vol. 47, pp. 35–52, 2006.

[7] T. Takeuchi, T. Ogawa, M. Nakagawa, and T. Kumagai, "Response evaluation of medium-span lattice domes with substructures using response spectrum analysis," in *Proceedings of IASS 2004*, (Montpellier, France), pp. 205–206, September 20-24 2004.

[8] The Building Standard Law of Japan on CD-ROM. *The Building Center of Japan, 2016.*

[9] E. L. Wilson, *CSI Analysis Reference Manual For SAP 2000, ETABS, SAFE and CSI Bridge*. Berkeley: Computer & Structures Inc, 2015.

[10] T. Takeuchi and A. Wada, *Buckling-Restrained Braces and Applications*. JSSI, 2017.

[11] X. Chen, T. Takeuchi, and R. Matsui, "Simplified design procedure for controlled spine frames with energy-dissipating members," *Journal of Constructional Steel*

Research, vol. 135, pp. 242–252, 2017. (DOI: 10.1016/j.jcsr.2017.04.017)

[12] K. Kasai, H. Ito, and A. Watanabe, "Peak response prediction rule for a SDOF elasto-plastic system based on equivalent linearization technique," *Journal of Structural and Construction Engineering (Transactions of AIJ)*, vol. 68, no. 571, pp. 53–62, 2003.

[13] A. K. Chopra, R. K. Goel, and C. Chintanapakdee, "Evaluation of a modified mpa procedure assuming higher modes as elastic to estimate seismic demands," *Earthquake Spectra*, vol. 20, no. 3, pp. 757–778, 2004. (DOI: 10.1193/1.1775237)

[14] T. Takeuchi, T. Kumagai, H. Shirabe, and T. Ogawa, "Seismic response evaluation of lattice roofs supported by multistory substructures," in *Shell and Spatial Structures: Structural Architecture - Towards the future looking to the past. IASS Symposium*, (Venice, Italy), p. 362, December 3-6 2007.

[15] T. Takeuchi, T. Ogawa, and T. Kumagai, "State-of-arts views on response control technologies on metal space structures," in *Proceedings of IASS 2009*, no. 6506, (Valencia, Spain), September 28-October 2 2009.

[16] K. Takamatsu, T. Takeuchi, T. Kumagai, and T. Ogawa, "Response evaluation of seismically isolated lattice domes using amplification factors," in *Proceedings of IASS 2009*, no. 6528, (Valencia, Spain), September 28-October 2009.

[17] X. Chen, T. Takeuchi, and R. Matsui, "Seismic performance and evaluation of controlled spine frames applied in high-rise buildings," *Earthquake Spectra*, vol. 34, no. 3, pp. 1431–1458, 2018. (DOI: 10.1193/080817EQS157M)